derived. During the tests, conditions of black space had to be simulated. The simulation was achieved by fixing a black faced shroud to a vacuum chamber cooled to −200°C using liquid nitrogen. The louvre blades were adjusted to operate within the required temperature range, i.e., closed at 10°C and fully open at 25°C. The heater operating temperature was slowly increased across this temperature range and the angular position of the louvre noted after thermal equilibrium was obtained for every setting of the heater temperature.

The test was repeated with the heater temperature reduced slowly across the same temperature range. This test was carried out to determine how closely the actuators followed the base temperature. The dynamic angular positional response of the louvre blades to a step input power of 20w to the heater was then studied till a steady state was obtained and the test was further repeated for a negative step input, also of 20w.

Experimental Results and Discussion

The test results are illustrated graphically. Figure 2 shows the power rejected by the array against the blade angle. A power rejection ratio in the open/closed position of 11:1, easily calculated from Fig. 2, was obtained which is a distinct improvement over the ratio 3:1 also shown in Fig. 2, before modifications described earlier were carried out.

In Fig. 3 is shown the variation of the base temperature, with the power rejected and shows how effectively the system controls the temperature for the large range of power—a function important in spacecraft application. Figure 3 also shows what temperatures would be obtained should the louvres either fail to open or close. In Fig. 4 is shown the dynamic response of the actuators to step inputs of power, either increasing or decreasing. In both cases the total response time is of the order of 90 min. It is also evident that about 4°C temperature difference between base and actuator is required before the latter begins to move but this settles to 1°C under steady-state conditions. This is possibly due to thermal lags and bearing friction. The shape of the response curves indicates slightly underdamped conditions.

References

[1] Russell, L. and Linton, R., "Experimental Studies of the Pegasus Thermal Control Louvre Array System," AIAA Paper 67-308, New Orleans, La., 1967.

[2] Clausen, O. W. and Kirkpatrick, J. P., "Thermal Tests of an Improved Louvre System for Spacecraft Thermal Control," AIAA Paper 69-627, San Francisco, Calif., 1969.

[3] Martin, P. and Yarworth, N., "An Introduction to the Theory and Use of Thermostatic Bimetals," *Engineering*, Vol. 192, 1961, p. 366.

Optimum Design of Elastomeric Gaskets for Combined Thermal and Vibration Performance

L. S. FLETCHER* AND T. E. SHOUP†
Rutgers University, New Brunswick, N.J.

Nomenclature

E = Young's modulus, psi
h_c = contact conductance coefficient, Btu/hr sq ft °F
Q/A = heat flux, Btu/hr sq ft
ΔR = attenuation, dB
ΔT = temperature difference °F
t = interstitial material thickness, in.
δ_0 = initial thickness between surfaces, μin.
ρ = density, lbm/ft^3
ω = vibration frequency, rad/sec

Subscripts
i = interstitial elastomer
mj = metallic junction

Received December 10, 1973; revision received January 22, 1974. This work was sponsored in part by the Research Council of Rutgers University.

Index categories: Heat Conduction; Structural Design, Optimal.

* Associate Professor of Aerospace Engineering. Member AIAA.
† Associate Professor of Mechanical Engineering.

Introduction

THE design and development of new spacecraft systems requires a continual re-evaluation and optimization of existing components. In order to optimize spacecraft components, problems associated with both thermal and vibration transmission across metallic junctions must be considered. Many of these junctions involve the use of elastomeric gaskets as a means of component sealing, thermal isolation or enhancement, and/or vibration isolation. These gaskets are often used in the miniaturization and refinement of electronic components which must be maintained at a present environment despite extreme temperature gradients, heat fluxes, and system vibrations. A schematic of the effect of elastomeric gaskets on these thermal and vibration characteristics is shown in Fig. 1.

These spacecraft optimization problems suggest the need for a new and more refined gasket design technique. Generally, design merit functions are established for the variables involved in a system. When these design merit functions are competitive, the usual compromise is to employ a tradeoff function. Occasionally, however, the merit functions are not in opposition and may be used to establish a truly optimum design. Such a situation arises in the design of elastomeric gaskets and a technique for use of these materials is presented in this Note.

Design Technique

Elastomeric materials are useful as gaskets because of their superior resistance to many types of environments, their excellent sealing capabilities, and their durability through repeated loadings. Selected neoprene, fluorocarbon, nitrile, polyacrylate, and silicone elastomers are considered in the present analysis. Many of these elastomeric materials contain various fillers to improve their mechanical or thermophysical properties. Elastomer fillers include such materials as carbon black, graphite, metallic flakes or powder, silica, and various oxides, as indicated in Table 1.

The thermal contact conductance of a junction with or without interstitial or gasket materials, provides a measure of the heat-

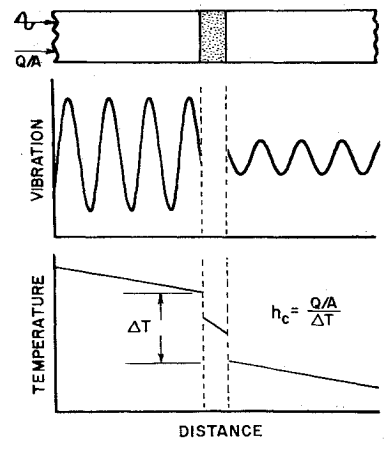

Fig. 1 Schematic of the effect of an elastomeric gasket on the thermal and vibration characteristics of a metallic junction.

Table 1 Elastomer material characteristics

Code	Elastomer material	Filler	Density lbm/ft^3	Youngs modulus, psi	Temperature range, °F	Thickness in.	ΔR^a_{max} decibels
N1	Neoprene	...	84.2	107424	−20–200	0.115	−38.17
IP1	Fluorocarbon D84-1[b]	Carbon black, etc.	117.2	284544	−40–500	0.082	−32.50
IP2	Nitrile EXN-117-3[b]	Graphite, Talc, etc.	90.5	193392	−40–300	0.078	−35.30
IP3	Silicone SIL-181-3[b]	Diatomaceous earth, peroxide, Iron Oxide	83.6	129888	−65–500	0.081	−37.38
IP4	Nitrile R36-1[b]	Carbon black, Organic peroxide	75.8	121536	−20–250	0.093	−38.09
IP5	Polyacrylate 4658-2[b]	Silica, Alumina Complex	84.9	116928	0–350	0.075	−37.76
C1	Silicone 1224[c]	Silver flakes	202.9	109440	−67–392	0.030	−34.27
C2	Silicone 1215[c]	Silver coated copper powder	227.9	129312	−67–257	0.028	−33.04
C3	Silicone X-4044-3[c]	Inorganic—dielectric, nontoxic thermally conductive material	109.3	219024	−67–392	0.017	−33.94
TW1	Silicone CONCIL R350[d]	Silver flakes	106.1	90720	−60–350	0.029	−37.90
TW2	Silicone CONCIL G600[d]	Silver flakes	112.3	125856	−60–350	0.028	−36.23
TW3	Silicone CONCIL G450[d]	Silver coated inert particles	106.1	138816	−100–400	0.029	−36.05
TW4	Silicone CONCIL G750[d]	Silver coated inert particles	112.3	200736	−100–400	0.030	−34.20

[a] Based on aluminum base material.
[b] International Packings Corporation, Bristol, N.H.
[c] Chomerics, Woburn, Mass.
[d] Technical Wire Products, Inc., Cranford, N.J.

transfer rate across a junction. Because of the lack of prediction techniques, these conductance data are generally determined experimentally in order to provide the necessary thermal design information for specific applications. Experimental thermal contact conductance data have recently been obtained for a range of selected elastomeric gasket materials,[1] and are used in the present analysis.

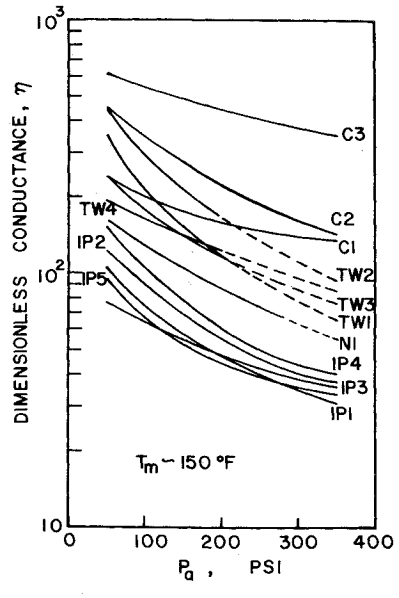

Fig. 2 Comparison of the dimensionless thermal conductance data for elastomeric gasket materials at a mean junction temperature of 150°F.

In order to extend the use of this experimental thermal conductance information to other cases, the data have been nondimensionalized. This dimensionless conductance or effectiveness of the gasket material has been defined[2] as the ratio of the thermal conductance of the elastomeric gasket material and thickness, to the bare metallic junction conductance and surface conditions, such that

$$\eta = (h_c t)_i/(h_c \delta_0)_{mj} \quad (1)$$

where δ_0 has been defined in terms of the surface flatness and roughness deviations.[2,3] The flattening of the gasket material has not been considered and will thus introduce a slight error into the over-all comparison. The effectiveness values of the elastomeric gasket materials listed in Table 1, are compared in Fig. 2 through use of the dimensionless conductance.

The magnitude of the dimensionless conductance permits the material selection of an optimum elastomeric gasket for a specific thermal application. A decreasing dimensionless conductance implies increasing effectiveness for thermal isolation applications. Conversely, the higher curves imply increased effectiveness for thermal dissipation.

In order to optimize the combined thermal and vibration performance of the elastomeric gaskets, it is necessary to determine their vibration or power attenuation characteristics. The power loss between members separated by a thin resilient layer is indicated in Fig. 1 and has been previously analyzed.[4,5] Assuming that the cross section area of the base material and the elastomeric gasket material are the same, the power attenuation in decibels can be determined as follows:

$$\Delta R = 10\log\left[\frac{1}{\cos^2[\omega t(\rho_i/E_i)^{1/2}]+\frac{1}{4}[(E\rho/E_i\rho_i)^{1/2}+(E_i\rho_i/E\rho)^{1/2}]^2\sin^2[\omega t(\rho_i/E_i)^{1/2}]}\right] \quad (2)$$

Inspection of this equation indicates that the attenuation will be zero decibels whenever the product of the wave number and elastomer thickness is $n\pi$, that is

$$\omega t(\rho_i/E_i)^{1/2} = n\pi \qquad n = 1,2,3,\ldots \quad (3)$$

and that the attenuation will have a maximum value whenever

$$\omega t(\rho_i/E_i)^{1/2} = (2n+1)\pi/2 \qquad n = 1,2,3,\ldots \quad (4)$$

The attenuation for this maximum value may be expressed in decibels as

$$\Delta R_{\max} = 20\log\left|\frac{2(E_i\rho_i E\rho)^{1/2}}{E_i\rho_i+E\rho}\right| \quad (5)$$

The maximum attenuation value is independent of material thickness and frequency for both maximum and minimum values, and the frequency at which it occurs is not dependent on material properties of the base material. Maximum values of attenuation predicted by Eq. (5) for the elastomers in contact with aluminum base material are listed in Table 1. A typical frequency response curve indicates that this resilient layer provides little attenuation for low frequencies and that as the frequency is increased, the maximum and minimum values repeat at integer multiples of the fundamental frequency. This is as expected in accordance with Eqs. (3) and (4).

Since the attenuation curves for the elastomeric materials are periodic between maximum and minimum values, they are not well suited for the attenuation of broad band noise. To overcome this shortcoming, two elastomer discontinuities could be used. These should be designed so that one has its maximum value while the other has its minimum value. In this way, the attenuation would be flat over a rather broad range. These two gaskets should be designed so as to be far enough apart (and separated by sufficient base material) to eliminate any possible dynamic interaction.

In order to select an elastomeric gasket material and thickness which permit maximum heat transfer and minimum vibration transmission, the following procedure would be used. The thermal characteristics are considered first, and the type of material is selected from Fig. 2 for the approximate joint loading. For a compression joint of 200 psi load and a gasket material with a nonmetallic filler, silicone elastomer *C*3 would be selected. The maximum vibration attenuation value ($\Delta R_{\max}$) for elastomer *C*3 is then read from Table 1. Equation (4) may then be used to determine the required thickness of this material for minimum vibration transmission. Once the thickness has been determined, the thermal conductance or effective thermal conductivity of the gasket may then be calculated with Eq. (1) and the bare junction characteristics.‡ The effectiveness of the vibration attenuation in the vicinity of the optimum design may then be determined from Eq. (2). Thus, the heat-transfer requirements give the selection of the material and the vibration requirements determine the thickness.

A technique for the optimum design and selection of elastomeric type gasket materials for combined thermal and vibration performance has been developed. The procedure has been demonstrated for the case of maximum heat transfer and minimum vibration transmission. The technique presented here may also be extended to applications involving the optimum design of gaskets for other materials and conditions.

‡ Effective bare junction thermal conductivity, $h_c\delta_0 = 0.0014P_a + 0.04$.

References

[1] Fletcher, L. S. and Miller, R. G., "Thermal Conductance of Gasket Materials for Spacecraft Joints," *AIAA Progress in Astronautics and Aeronautics: Thermophysics and Spacecraft Thermal Control*, Vol. 35, edited by R. G. Hering, MIT Press, Cambridge, Mass., 1974.

[2] Fletcher, L. S., "A Review of Thermal Control Materials for Metallic Junctions," *Journal of Spacecraft and Rockets*, Vol. 9, No. 12, Dec. 1972, pp. 849–850.

[3] Fletcher, L. S. and Gyorog, D. A., "Prediction of Thermal Contact Conductance Between Similar Metal Surfaces," *AIAA Progress in Astronautics and Aeronautics: Heat Transfer and Spacecraft Thermal Control*, Vol. 24, edited by J. W. Lucas, MIT Press, Cambridge, Mass., 1971, pp. 273–288.

[4] Kenner, V. H. and Goldsmith, W., "One-Dimensional Wave Propagation Through a Short Discontinuity," *Journal of the Acoustical Society of America*, Vol. 45, No. 1, 1969, pp. 115–118.

[5] Beranek, L. L., *Noise and Vibration Control*, McGraw-Hill, New York, 1971, pp. 252–355.

Computer Illustrations of Earth Satellite Orbits

DONALD L. HITZL*

Lockheed Palo Alto Research Laboratory, Palo Alto, Calif.

Introduction

IN most forms of analytical work, there is often a dichotomy between those who rely on clever paper and pencil analysis and those who rely on extensive simulation by computer. However, computer illustrations, which combine rapid visualization with numerical precision, can form a natural bridge between these two viewpoints. Moreover, the importance of visual information in general, and for aerospace applications in particular, should not be underestimated.[1]

As an example of visual results, a set of computer-generated plots are presented which show the orbital motion and ground track for satellites in various Earth orbits. Since most Earth satellite applications involve the orbital motion with respect to some geographical area or location on the Earth's surface, the plots depict satellite motion *relative* to the rotating Earth. The orbits shown are all Keplerian ellipses with prescribed eccentricities and periods. However, as a result of the superimposed rotation of the Earth, the simple two-body motion is distorted in unusual (and sometimes unexpected) ways.

Table 1 Orbit elements

Orbit elements	Orbit period T (hr) 6	8	12	24
semimajor axis a (naut miles)	9046.71	10959.32	14360.79	22796.39
eccentricity[a] e	0.509	0.595	0.5	0.1
inclination i (deg)	63.4	63.4	63.4	63.4
argument of perigee ω (deg)	−90.0	−90.0	−90.0	−90.0
right ascension of ascending node Ω (deg)	−90.0	−90.0	−110.0	90.0
mean anomaly at initial time $M(t_0)$ (deg)	0.0	0.0	35.19	0.0

[a] Note that the eccentricities for the 6- and 8-hr orbits were chosen so perigee altitude would be 1000 naut miles.

Received August 2, 1973; revision received January 15, 1974. Help with the computer program generously given by the late K. Shoop is gratefully acknowledged. This material was developed in the course of satellite systems studies sponsored by the Department of the Air Force.

Index categories: Earth-Orbital Trajectories; Earth Satellite Systems, Unmanned; Computer Technology and Computer Simulation Techniques.

* Research Scientist, Mathematics and Systems Analysis Department. Member AIAA.